JOURNAL OF ENVIRONMENTAL SCIENCES 124 (2023) 875–891

Available online at www.sciencedirect.com

ScienceDirect

www.elsevier.com/locate/jes

JES JOURNAL OF ENVIRONMENTAL SCIENCES

www.jesc.ac.cn

Integration of chemical fractionation, Mössbauer spectrometry, and magnetic methods for identification of Fe phases bonding heavy metals in street dust

Beata Górka-Kostrubiec[1], *Ryszard Świetlik*[2], *Tadeusz Szumiata*[3], *Sylwia Dytłow*[1,*], *Marzena Trojanowska*[2]

[1] *Institute of Geophysics, Polish Academy of Sciences, ks. Janusza 64, 01-452 Warsaw, Poland*
[2] *Department of Environmental Chemistry and Engineering, University of Technology and Humanities in Radom, 27 Bolesława Chrobrego Str., 26-600 Radom, Poland*
[3] *Department of Physics, Faculty of Mechanical Engineering, University of Technology and Humanities in Radom, 54 Krasickiego Str., 26-600 Radom, Poland*

ARTICLE INFO

Article history:
Received 5 March 2021
Revised 9 February 2022
Accepted 10 February 2022
Available online 24 February 2022

Keywords:
Heavy metals
Street dust
Chemical fractionation
Magnetic methods
Mössbauer spectrometry

ABSTRACT

Street dust is one of the most important carriers of heavy metals (HMs) originating from natural and anthropogenic sources. The main purpose of the work was to identify which of Fe-bearing phases bind HMs in street dust. Magnetic parameters of the Fe-bearing components, mainly magnetically strong iron oxides, are used to assess the level of HM pollution. Chemical sequential extraction combined with magnetic methods (magnetic susceptibility, magnetization, remanent magnetization) allowed determining the metal-bearing fractions and identifying the iron forms that are mostly associated with traffic-related HMs. The use of Mössbauer spectrometry (MS) supplemented by magnetic methods (thermomagnetic curves and psarameters of hysteresis loops) enabled precise identification and characterization of iron-containing minerals. The classification of HMs into five chemical fractions differing in mobility and bioaccessibility revealed that iron is most abundant (over 95%) in the residual fraction followed by the reducible fraction. HMs were present in reducible fraction in the following order: Pb>Zn>Mn>Cr>Ni>Fe>Cu, while they bound to the residual fraction in the following order: Fe>Ni>Cr>Mn>Pb>Cu>Zn. The signature of the anthropogenic origin of street dust is the presence of strongly nonstoichiometric and defected grains of magnetite and their porous surface. Magnetite also occurs as an admixture with maghemite, and with a significant proportion of hematite. A distinctive feature of street dust is the presence of metallic iron and iron carbides. Magnetic methods are efficient in the screening test to determine the level of HM pollution, while MS helps to identify the iron-bearing minerals through the detection of iron.

© 2022 The Research Center for Eco-Environmental Sciences, Chinese Academy of Sciences. Published by Elsevier B.V.

* Corresponding author.
E-mail: skdytlow@igf.edu.pl (S. Dytłow).

https://doi.org/10.1016/j.jes.2022.02.015
1001-0742/© 2022 The Research Center for Eco-Environmental Sciences, Chinese Academy of Sciences. Published by Elsevier B.V.

Introduction

In an urban environment, street dust is considered as one of the most important carriers of heavy metals (HMs) (Sutherland, 2003; Padoan et al., 2017) originating from natural and anthropogenic sources. Its primary anthropogenic source is exhaust and nonexhaust traffic-related emission, resulting from fuel burning, wear of different parts of vehicles (e.g. tires and brake pads) and vehicle body rust, leakage of brake and lubricating oil, and abrasion of the road surface and road paint (Khanal et al., 2014; Li et al., 2015; Yildirim and Tokalioğlu, 2016). The introduction of new technologies by automobile companies has significantly reduced the contribution of tailpipe emissions to total traffic-related pollution. However, even with the introduction of modern electric and hybrid vehicles, a reduction in nonexhaust emissions, which result from the physical phenomena associated with vehicle movements, has not been achieved. Nonexhaust emission cannot be ignored due to its increasing contribution to total dust as well as its link with toxic metals that have health consequences Harrison et al. (2012). estimated that the wear of brake pads contributing to almost 55% of the emission of <10 µm particulate matter mass is the main source of nonexhaust emissions. Nowadays, in order to ensure optimal braking conditions for faster vehicles, automobile manufacturers use modern braking systems containing various chemical compounds, which are often enriched with metals that are toxic to the environment and human health (Hwang et al., 2016; Jadhav and Sawant, 2019).

In many studies, street dust as a carrier of HMs has been considered as a valuable indicator of the quality of an urban environment (Shi et al., 2011) and used for assessing the risk of HMs for human health (Keshavarzi et al., 2015; Li et al., 2017; Gope et al., 2018; Trojanowska and Świetlik, 2020). However, only sporadic research focuses on the chemical fractionation of HMs in the solid phase of dust, although this approach can provide useful information on the mobility and bioavailability of pollutants in the environment, Świetlik et al. (2015) emphasized that the mobility, biological availability, and toxicity of HMs are not only directly linked to their concentration. The knowledge of their abundance in physical and chemical forms is more critical than providing their total concentration in environmental samples. Metals contained in the solid phase of street dust are bound in various chemical fractions, of which the most frequently indicated are carbonates, sulfides, organic matter, iron oxides, aluminum and manganese oxyhydroxides and phyllosilicate minerals (Świetlik et al., 2015; Adamiec, 2017). Chemical fractionation carried out through multistage extraction using progressive aggressiveness reagents is one of the ways for the speciation of metals in environmental samples. Knowledge of the fractions of metals bound to different solid phases of street dust is essential not only for understanding the mode of occurrence and mobility of traffic-related metals but also for identifying their sources.

The pollutants released by anthropogenic urban and industrial activities, including nonexhaust vehicle emissions, contain significant amounts of iron-bearing components with ferromagnetic (*sensu lato*) and paramagnetic properties (Muxworthy et al., 2002; Christoforidis and Stamatis, 2009; Zhang et al., 2016). This means that dust particles can be examined, characterized, and identified by their specific physical properties using magnetic methods and Mössbauer spectrometry (MS), a technique dedicated to precise recognition and differentiation of iron-rich minerals. An additional characteristic feature of the anthropogenic iron forms of street dust is their coexistence with HMs, and thus, the magnetic parameters proportional to the content of magnetic particles are used for the quantification of HMs as well as for assessing the level of HM pollution. On the other hand, the Mössbauer technique is critical in identifying Fe-rich phases which, according to many works, appear to be an indicator of nonexhaust emissions in street dust (Muxworthy et al., 2002; Szumiata et al., 2013). The Fe-rich phases including goethite, lepidocrocite, magnetite, and hematite are corrosion products formed on iron and low-alloy steels, while magnetite, the most common contributor to street dust, is additionally generated by the abrasion or corrosion of engine body material (Harison et al., 2012; Grigoratos and Martini, 2015). It was found that the main source of iron is the wear of brake blocks and bearings, while the abrasion of brake discs also results in the production of Mn and Cu apart from Fe.

The main purpose of the work was to identify which of Fe-bearing phases bind HMs in street dust. This is a very essential topic problem, as magnetic parameters of the Fe-bearing minerals, are used to assess the level of traffic-related HM pollution. In this study, correlations of magnetic parameters, such as magnetic susceptibility and magnetization, with metal-bearing iron fractions determined by the chemical sequential extraction method indicated the iron forms that are mostly associated with traffic-related HMs (Cr, Cu, Fe, Mn, Ni, Pb, and Zn) and the magnetic signature of minerals. The chemical and magnetic analyses were performed depending on the size of the granulometric fractions of dust: for a coarse-grained fraction (1000–60 µm) and for a fine-grained fraction (<63 µm) which is very harmful and exhibits adverse effects on human health. According to the results reported by Adamiec et al. (2016) and Grigoratos and Martini (2015), about 90% of all the metals originating from brake pads contribute to the <20 µm fraction of nonexhaust traffic emission.

Another important goal of this work was the precise identification and characterization of iron-containing compounds using MS supplemented by magnetic methods. ^{57}Fe transmission MS (both at room and liquid nitrogen (LN) temperature) is a specially dedicated method, which has so far been very effectively utilized in the investigations of various kinds of urban and industrial dust. It allows distinguishing the Fe-bearing minerals even if they occur in relatively small amounts and/or exhibit weak magnetic properties difficult to be identified by magnetic methods. In the frame of this work, it was also checked if the hyperfine parameters of Mössbauer spectra could be a reliable indicator of an anthropogenic and soil-based component of street dust.

1. Materials and methods

1.1. Sampling area

Radom is a medium-sized postindustrial town (112 km^2 in area with 215,000 inhabitants) located in central Poland (**Fig. S1**) (51°24.1518′N, 21°8.8284′E) in a typical agricultural region away from industrial emission sources of HMs (GUS Report, 2018). It is the place of intersection of the main international and state traffic routes connecting east with west and north with south of Poland. The local sources of HM emission are vehicle traffic, domestic coal combustion, coal-fired municipal heating plants, metalworking plants, tanneries, a cigarette manufacturing plant, and factories manufacturing household and cosmetic products (Mordak et al., 2008). For this study, street dust samples were collected in four sites (P-I, P-II, P-III, and P-IV) that differ in the levels of air pollution (Airly, https://airly.eu/map/pl) and traffic intensity (The Programme, http://www.radom.pl):

- P-I: 1905 Roku Street (maximum traffic intensity: 2,100 veh/hr), old industrial district, currently one of the main Radom arteries—section of national road No. 12;
- P-II: NSZ Roundabout—E77 driveway to Radom (maximum traffic intensity: 2,500 veh/hr), suburban, blocks of flats;
- P-III: Matki Boskiej Fatimskiej Roundabout—E371 exit road (maximum traffic intensity: 1,100 veh/hr), suburban, scattered housing; and
- P-IV: Kielecka Street, transit road E77 (maximum traffic intensity: 2,500 veh/hr), suburban, scattered housing.

1.2. Collection of samples

The samples for the study were collected during the dry season between May and June in 2015 using a clean plastic dustpan and a brush, from the lane adjacent to the edge of the road along a 10-m stretch. To avoid resuspension of very fine particles during sampling, sweeping was done slowly and the samples were directly transferred into plastic bags. About 500 g of samples was collected at each sampling point and mixed thoroughly to obtain a bulk sample. Each sample was air-dried to a constant weight and sieved through a 1-mm nylon sieve to remove stones, coarse material, plastic, and other impurities. The dried samples were sieved again through a 63-µm sieve to isolate a fine fraction of street dust, which potentially poses the greatest threat to human health (Li et al., 2017). Depending on the location, the coarse granulometric fraction (1 mm≥d>63 µm in diameter) of dust was marked as P-IB, P-IIB, P-IIIB, and P-IVB, while the fine granulometric fraction (≤63 µm in diameter) was marked as P-IA, P-IIA, P-IIIA, and P-IVA. All the samples were stored in plastic bags and placed in tightly closed plastic containers before the analysis.

1.3. Chemical methods

1.3.1. Reagents

All reagents used were at least of analytically pure grade: CH_3COONa (POCh, Poland) pure p.a., CH_3COOH 100% (Merck, Germany) extra pure, $NH_2OH{\cdot}HCl$ (POCh, Poland) pure p.a., CH_3COONH_4 (POCh, Poland) pure p.a., HNO_3 65% (Merck, Germany) Suprapur, and H_2O_2 (Chempur, Poland) pure p.a. The solutions were prepared with deionized water purified by Millipore System (Milli Q-Plus, USA) to a resistivity of 18.2 MΩ cm.

1.3.2. Microwave-assisted digestion

The environmentally available concentration of HMs in the street dust (i.e. pseudo-total concentration of HMs) was determined via microwave-assisted digestion of the samples using concentrated HNO_3 and 30% H_2O_2 according to the manufacturer's protocol (Millestone, 1992). Samples were heated according to a five-step program: 1) 250 W, 6 min; 2) 0 W, 1 min; 3) 400 W, 6 min; 4) 650 W, 6 min; and 5) 250 W, 6 min. The digests were transferred quantitatively into 50-cm^3 calibrated flasks. Three subsamples were digested simultaneously for each sample of street dust.

1.3.3. Sequential extraction

Fractionation of samples was carried out by following the modified Tessier's five-step extraction scheme (**Table 1**) (Tessier et al., 1979), as described by Trojanowska and Świetlik (2020). The F(1) fraction was defined as a water-soluble fraction. The next three fractions were extracted according to the original method of Tessier et al. (1979), but in view of the strongly "artificial" nature of street dust, the terminology used in this work was based on the operational characteristic of chemical fractionation (Ure and Davidson, 2002). Thus, the F(2) fraction (defined by Tessier as a fraction associated with carbonates) was a weak acid-soluble fraction, F(3) (defined as a fraction associated with Fe/Mn-oxides) a reducible fraction, and F(4) (defined as a fraction associated with sulfides and organic matter) an oxidizable fraction. The residual fraction F(5) was extracted using a mixture of concentrated HNO_3 and 30% H_2O_2 under the same conditions as applied for determining the pseudo-total metal content. Chemical fractionation was conducted for three subsamples of each sample.

1.4. Metal determination in chemical fractions

The concentration of Cr, Cu, Fe, Mn, Ni, Pb, and Zn in the extracts after the microwave-assisted digestion and in the extracts after each step of sequential extraction were determined using atomic absorption spectrophotometry (Agilent Technologies 200 Series AA 240 FS AA, USA) with flame atomization. Standard solutions of metals prepared by appropriate dilution of the stock solution (1000 µg/mL, BDH Spectrosol) were used to calibrate the spectrophotometer using the standard curve method. All the measurements were performed in triplicate. The detection limits for the examined metals were as follows: Cr-0.04 mg/dm^3; Cu-0.04 mg/dm^3; Fe-0.10 mg/dm^3; Mn-0.06 mg/dm^3; Ni-0.03 mg/dm^3; Pb-0.09 mg/dm^3; and Zn-0.03 mg/dm^3.

1.5. Contamination factor and pollution load index

The contribution of HMs to the overall toxicity status of street dust was analyzed using the pollution load index (PLI), proposed by Tomlinson et al. (1980). PLI is defined as the n-th root

Table 1 – Sequential extraction procedure [a], [b].

Fraction		Reagent	Volume	Time	Temperature.
F(1)	Water soluble	H_2O	10 mL	24 hr	25°C ± 2°C
F(2)	Weak acid soluble	1 mol/L NaOAc, pH 5 (HOAc)	8 mL	5 hr	25°C ± 2°C
F(3)	Reducible	0.04 mol/L $NH_2OH·HCl$ in 25% HOAc	20 mL	6 hr	96°C ± 2°C
F(4)	Oxidizable	30% H_2O_2 (pH 2) + 0.02 mol/L HNO_3;	5 mL + 3 mL	2 hr	85°C ± 2°C
		30% H_2O_2 (pH 2);	3 mL	3 hr	85°C ± 2°C
		3.2 M NH_4OAc in 20% HNO_3	5 mL	30 min	25°C ± 2°C
F(5)	Residual	65% HNO_3 + 30% H_2O_2	5 mL + 1 mL	microwave-assisted, analogously as pseudo-total content determination	

[a] 1.00 g of sample was used
[b] All extracted solutions were separated by centrifugation at 10,000 rpm for 30 min and filtered through a membrane filter Millipore 0.45 µm

of multiplication of the contamination factor (CF_n):

$$PLI=\sqrt[n]{CF1 \times CF2 \times \ldots. \times CFn} \quad (1)$$

where, CF_n is the ratio obtained by dividing the concentration of the n-th element (C_n given in mg/kg) by its corresponding background value (B_n). PLI was calculated based on the geochemical background values of the metal concentration in Polish soils (Czarnowska, 1996). It is accepted that PLI values >1 indicate anthropogenic sources of elements, whereas values <1 indicate a nonpolluted level.

1.6. *Magnetic methods*

1.6.1. *Magnetic susceptibility and anhysteretic remanent susceptibility*

Magnetic susceptibility describes the ability of a material to change its magnetization when influenced by an external magnetic field. It is depended on the content of magnetic particles, their mineralogy, and grain-size distribution (Thompson and Oldfield, 1986). Magnetic susceptibility is used in environmental studies as a proxy of the content of anthropogenic magnetic particles (AMPs), the presence of which is usually associated with HMs. Low-field volume magnetic susceptibility (κ) was measured with a sensitivity of 2×10^{-8} SI, at two frequencies (976 and 15,600 Hz) of a magnetic field with an intensity of H=200 A/m, using a Multi-Function-Kappabridge MFK1-FA (AGICO, Brno, Czech Republic). Each measurement was repeated three times, and the average κ value was calculated. In environmental studies, low-field mass-specific magnetic susceptibility (χ) is more commonly used. It refers to the volume magnetic susceptibility normalized by a sample mass, which was measured with a significance of ±1 mg using an analytical balance.

The anhysteretic remanent magnetization (ARM) was acquired at 100 mT of an alternating-current magnetic field and 100 µT of a direct-current (DC) magnetic field using the LDA-3 device (AGICO, Brno Czech Republic) and was measured by a SQUID magnetometer (2G Enterprises, Sunnyvale, CA, USA). The anhysteretic remanent susceptibility (χ_{ARM}) was calculated by dividing the value of ARM by the value of the DC bias magnetic field. This parameter is used to discriminate between the grain-size distributions of magnetic particles, particularly in terms of the contribution of single-domain (SD) grains in the size range of 0.03–0.08 µm (Moskowitz, 2007).

1.6.2. *Hysteresis parameters*

The hysteresis parameters and their appropriate ratios can be used to determine the mineralogy type and the content of magnetic minerals, as well as the dominant magnetic grain size expressed by the domain state of magnetic particles (Maher, 1998). The saturation magnetization (M_s), saturation remanence (M_{rs}), and coercive field B_c were determined from the hysteresis loop after subtracting the high-field linear trend. The values of M_s and M_{rs} were normalized by the mass of the sample. The curve of subsequent DC back-field demagnetization of isothermal remanent magnetization (IRM) was used for the determination of the coercivity of remanence (B_{cr}). B_{cr} is a field, opposite to saturation of IRM (SIRM), necessary to decrease the remanence to zero. The hysteresis loops and the curves of the DC back-field were measured with an alternating gradient magnetometer (MicroMag AGM 2900; Princeton Measurement Corporation, Princeton, NJ, USA) which was operating at a maximum magnetic field of 1 T.

1.6.3. *Thermomagnetic curves of κ(T) and M(T)*

The temperature changes of magnetic susceptibility (κ(T) curve) and induced magnetization (M(T) curve) were applied for identifying the magnetic minerals by estimating their characteristic Curie/Néel temperatures. The curves of κ(T) were measured in an air atmosphere by the Kappabridge KLY-3 (AGICO, Brno, Czech Republic) coupled with the CS-3 high-temperature furnace over a temperature range of 30°C–700°C. Curie temperature (T_C) was calculated using the differential method based on the inflexion point on the decreasing branch of κ(T) curve, at which the paramagnetic behavior starts to dominate (Petrovský and Kapička, 2006). The M(T) curves were measured in free air using an advanced variable field translation balance (MAG Instruments, Munich, Germany), at 30°C–800°C, in a magnetic field of 500 mT, which was enough to saturate the samples. The M(T) values were measured for the usual samples of street dust and their magnetic extracts separated by neodymium hand-magnet.

1.7. Statistical analysis

All the graphs were statistically analyzed and plotted using Origin 8.6 software (OriginLab Corp., USA) and Microsoft Excel 2019. Correlation between the magnetic parameters and the metal concentrations was determined by Pearson's correlation coefficient, and the level of significance was set at $p<0.001$.

1.8. Mössbauer spectrometry

^{57}Fe transmission MS was used to determine the mineralogy of iron-containing phases (both ferrimagnetic and paramagnetic) and to revalidate the iron speciation results obtained with chemical methods. All samples were measured at room temperature with a spectrometer produced by POLON (Poland) and modernized at University of Technology and Humanities (UTH) in Radom, Poland. The spectometer was arranged in vertical configuration and equipped with a ^{57}Co(Rh) radioactive source (activity = 0.7 GBq) as well as a vibrator operating in constant acceleration mode. A proportional counter was utilized for detecting the radiation transmitted through the sample. The automatic system was responsible for counting gamma quanta in correlation with the source velocity offering the spectra resolution of 512 channels (after folding). To maintain the unchanged proportions of the mineralogical phases, the samples were not magnetically separated or concentrated. As a result, long-time measurements (usually several days per sample) were needed for providing satisfactory statistics of the Mössbauer spectra (even over 20 million counts per channel in a folded spectrum). In the case of one sample, the additional low-temperature measurements were carried out for better identification of the superparamagnetic phases, using a horizontally arranged spectrometer with a vertical cold finger immersed in LN. The achieved working temperature of this sample was about 91 K.

The Mössbauer spectra were fitted using the freeware PolMöss package (by T. Szumiata). This dedicated Microsoft Excel workbook with Solver extension provides both gradient and genetic optimization algorithms implemented for multicore processors. The software enables convoluting the Lorentzian baselines with Gaussian distributions of hyperfine parameters, resulting in a Voigt profile of fitted subspectra. The PolMöss package has been effectively applied for the Mössbauer analysis of various environmental and geological samples, such as highway dust (Szumiata et al., 2013), fly ashes (Szumiata et al., 2015), industrial dust (Szumiata et al., 2017), and meteorites (Bogusz et al., 2018).

2. Results and interpretation

2.1. Heavy metal concentrations and distribution of iron in chemical fractions of street dust

The pseudo-total concentrations of Fe, Cr, Cu, Mn, Ni, Pb, and Zn determined for the street dust samples are listed in Table 2. The highest concentrations of all the studied HMs (Cr-66.0 mg/kg, Cu-305.0 mg/kg, Fe-22,860 mg/kg, Mn-631.0 mg/kg, Ni-76.7 mg/kg, Pb-108.0 mg/kg, and Zn-726.0 mg/kg) were observed in the fine fraction. The coarse fraction was severalfold less enriched with HMs (from 2.5 times for Fe to 6.8 times for Zn) compared to the fine fraction.

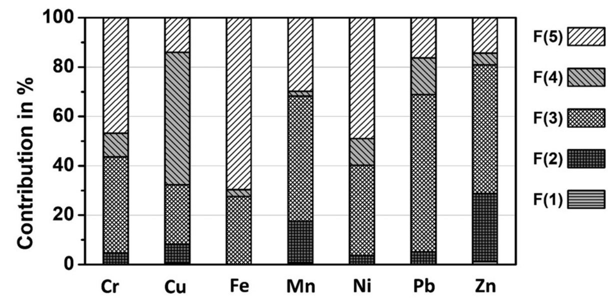

Fig. 1 – Average percentage contribution of traffic-related heavy metals to the five chemical fractions of street dust.

The high positive correlations between the groups of individual HMs can be indicative of the similarity of their primary emission sources (Table 3). Very strong and positive correlations were found between Cu, Fe, Mn, and Zn in the first group ($r_{Mn/Zn}$=0.99, $r_{Fe/Cu}$=0.97, $r_{Fe/Mn}$=0.97, $r_{Fe/Zn}$=0.97, $r_{Cu/Mn}$=0.95, $r_{Cu/Zn}$=0.95; p=0.001, N=8) and between Cr, Ni, and Pb in the second group ($r_{Cr/Pb}$=0.97, $r_{Ni/Cr}$=0.96, $r_{Ni/Pb}$=0.95; p=0.001, N=8). This result can indicate the emission of HMs from various sources but belonging to one category (e.g. wear of body parts of a car and exhaust emissions, both resulting from motion vehicles). In the first group, the relevance of exhaust emission in the distribution of Fe, Cu, Mn, and Zn metals was probably limited, whereas in the second the exhaust emission could significantly determine the distribution of Cr, Ni, and Pb in street dust. It is worth emphasizing that the first group of metals regarded as originating from wear emission was used as a key tracer in the calculations of brake wear emission by Grigoratos and Martini (2015).

The average percentage contribution of individual HMs to the five chemical fractions (the contribution of HMs to the F(1) fraction was in most cases below the detection limit) varied greatly as depicted in Fig. 1. Two chemical fractions, residual F(5) and reducible F(3), were the most abundant in Fe. They bound over 95% of the total concentration of Fe occurring in street dust. The contribution of Cu varied from 7.8% to 52.7% with the greatest input to the oxidizable fraction F(4), while the lowest content accounting for 8.7% was observed in the weak acid-soluble fraction F(2). An amount of 15.0% and 24.1% was associated with the residual fraction F(5) and reducible fraction F(3), respectively. Compared with other HMs, Cu was the primary contributor to the oxidizable fraction F(4). The capacity of Cu to be bound to organic matter and sulfide has been widely described by other authors (Li et al., 2001; Yang et al., 2006). The highest contribution of Ni (49.5%) was found in the F(5) fraction, while the contribution to F(2), F(4), and F(3) fractions accounted for 3.6%, 10.9%, and 36.0%, respectively. The highest content of Ni was also found in the residual fraction of street dust and roadside soils by Banerjee (2003) and Lee et al. (2005). Pb was dominant in the reducible fraction (62.8%); its contribution to F(4) and F(5) fractions was 14.8% and 17.3%, respectively, while in F(2), it was found to be of secondary importance Sutherland and Tack (2000)., Li et al. (2001),

Table 2 – Pseudo-total concentrations of heavy metals in street dust.

ID sample	Pseudo-total concentration of heavy metals (mg/kg)							PLI	χ x 10^{-8} (m^3/kg)
	Cr	Mn	Ni	Pb	Zn	Fe	Cu		
Background	27	289	10.2	9.8	30	12900	7.1		
P-IA	66.0	475.0	76.7	108.0	505.0	18530	164.0	5.7	452.4
P-IIA	55.1	601.0	44.8	75.5	627.0	22860	271.0	5.7	547.1
P-IIIA	47.4	631.0	41.8	93.2	726.0	21800	305.0	5.9	614.1
P-IVA	45.7	536.0	37.3	72.2	632.0	19670	208.0	5.0	548.0
P-IB	22.8	96.0	12.2	15.8	50.2	7500	23.9	1.1	105.8
P-IIB	19.2	158.0	13.6	13.5	131.0	12250	124.0	1.8	263.2
P-IIIB	13.9	152.0	10.9	11.0	77.0	6260	41.3	1.1	180.0
P-IVB	11.2	137.0	12.3	14.1	106.0	7100	38.3	1.2	151.3
Pearson's correlation coefficients of individual heavy metal concentration with magnetic parameters									
χ	0.84	0.99	0.74	0.89	0.99	0.98	0.97	0.97	
M_s	0.83	0.99	0.71	0.88	0.98	0.95	0.96		
M_{rs}	0.81	0.94	0.65	0.82	0.94	0.92	0.91		

PLI - pollution load index, χ - mass-specific magnetic susceptibility; M_s - saturation magnetization; M_{rs} - remanent magnetization and correlation coefficients of individual heavy metals with magnetic parameters: χ, M_s and M_{rs}.
Background values for heavy metals according to Czarnowska (1996).

Table 3 – Pearson's correlation coefficients between pseudo-total concentration of individual traffic-related heavy metals in street dust.

	Cr	Cu	Fe	Mn	Ni	Pb	Zn
Cr	1	0.77***	0.89**	0.88**	0.96*	0.97*	0.86**
Cu		1	0.97*	0.95*	0.64	0.82***	0.95*
Fe			1	0.97*	0.77***	0.89**	0.97*
Mn				1	0.77***	0.92**	0.99*
Ni					1	0.95*	0.76***
Pb						1	0.92**
Zn							1

* Correlation is significant at the 0.001 level (two-tailed).
** Correlation is significant at the 0.01 level (two-tailed).
*** Correlation is significant at the 0.05 level (two-tailed).

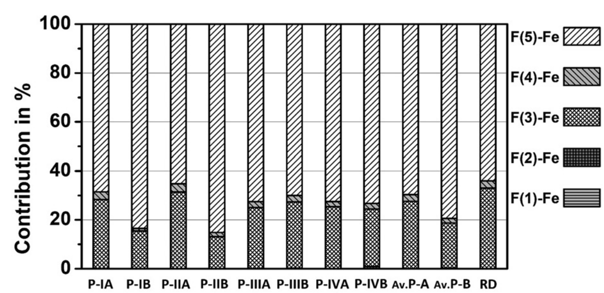

Fig. 2 – Chemical fractionation pattern of iron in individual street dust samples: P-IA, P-IB, P-IIA, P-IIB, P-IIIA, P-IIIB, P-IVA, and P-IVB; averages for a fine-grained fraction (Av. P-A) and coarse-grained fraction (Av. P-B), and for road dust retained on noise barriers along expressway (RD) according to Świetlik et al. (2015).

and Yang et al. (2006) reported that the association of Pb with the reducible fraction resulted from its ability to form stable complexes with Fe and Mn oxides. The reducible fraction was most abundant in Zn (52.2%), followed by F(2) with an average contribution of 27.3% and then by the residual fraction with 14.3%. The oxidizable fraction had only a minor amount of Zn (4.8%). It was shown by Ramos et al. (1994) that the presence of Zn in the F(2) fraction as bound to carbonates was directly related to the optimal pH for metal precipitation in soils. Manganese was primarily bound to F(3) (50.2%), followed by F(5) (29.8%) and F(2) (17.5%) fractions, with the smallest percentage (2%) found in F(4). The average percentages of Cr fractions were in the following order: F(5) (46.7%)>F(3) (39.2%)>F(4) (9.5%)>F(2) (4.6%).

The result of fractionation of iron into five chemical fractions differing in mobilities and bioaccessibilities is shown in Fig. 2. Data are presented for the individual studied sites depending on the size of the granulometric fractions of dust. Iron was most abundant in the residual fraction F(5)-Fe followed by the reducible fraction F(3)-Fe, which is in line with the study of Keshavarzi et al. (2015) and Gope et al. (2018). The average percentage contribution of F(5)-Fe in the coarse granulometric fractions (78.0%±3.7%) was higher than the fine granulometric fraction of these samples (69.7%±1.8%) and in contrast, the average percentage contribution of F(3)-Fe in the fine fraction (27.5%±1.5%) was higher than in the coarse fraction of these samples (19.8%±3.3%). The oxidizable and weak acid-soluble fractions bound much less iron, accounting for, on average, 2.4% and 0.2%, respectively. The content of water-soluble Fe species (free ions or complexed ions) was less than the limit of detection of the analytical procedure (3.8 mg/kg). The iron distribution pattern in street dust was found to be very similar to that in road dust retained on noise barriers along expressway by Świetlik et al. (2015) (Fig. 2; bar marked as RD).

2.2. Magnetic parameters and their correlations with chemical speciation of metal-bearing forms in street dust

Figure S2 presents the histograms of magnetic parameters-χ, M_s, and M_{rs}-which quantify the magnetic minerals in coarse and fine granulometric fractions of street dust. The values of these parameters are listed in **Table S1**. All the parameters showed almost a similar trend based on the granulometric fractions; in general, the higher values were always observed in the fine-grained fraction. This finding is analogous to the results of chemical analyses, which showed that the fine granulometric fraction was highly enriched in HMs (Table 2). The magnetic susceptibility, commonly used for the quantification of AMPs, ranged from 452.4 to 614.1×10^{-8} m^3/kg in the fine-grained fraction, and from 105.8 to 263.2×10^{-8} m^3/kg in the coarse-grained fraction. The most significant differences in χ values between the grain-size fractions were observed for sampling site P-I, in which the value of χ for P-IA was about 4.5 times higher than for P-IB. For fine- and coarse-grained fractions collected from location P-IV, the values of M_s and M_{rs} were about 4 and 5.5 times higher, respectively.

The coefficients of correlations between χ, M_s, and M_{rs} and the pseudo-total concentrations of HMs are listed in Table 2. Among the three studied magnetic parameters, magnetic susceptibility showed the strongest correlation with HMs ($r_{Cr}=0.80$, $r_{Mn}=0.99$, $r_{Ni}=0.74$, $r_{Pb}=0.89$, $r_{Zn}=0.89$, $r_{Fe}=0.98$, and $r_{Cu}=0.97$) (Table 2). These results indicate the existence of significant relationships between the magnetic signature and HM concentrations in street dust. It is not surprising due to the fact if iron content strongly correlates with magnetic susceptibility, as presented in Table 2, and simultaneously with individual HMs (Table 3), then it can be expected that magnetic susceptibility will also correlate well with HM contents (Table 2). The contribution of HMs to the overall toxicity status was analyzed using PLI (**Fig. S2d**), with values >5 obtained for the fine-grained fraction, indicating a high pollution level. It is apparent from Table 2 that *PLI* strongly correlates with χ, with a Pearson's linear coefficient of 0.93 ($p<0.001$). It confirms that magnetic susceptibility not only acts as a useful parameter for assessing the level of pollution by individual HMs but also reflects their collective impact estimated by PLI.

An important aim of this study is to find out which iron species coexisting with traffic-related HMs mainly contribute to the magnetic properties of street dust. Therefore, the relationship between χ the concentration of Fe (Fig. 3**a**), and the contribution of HMs to F(3) and F(5) (Fig. 3**b**) fractions was analyzed in detail. It is clear on one hand that the magnetic susceptibility very well correlates with iron content (Fig. 3**a**) and on the other that two chemical fractions bearing together >95% of iron content are responsible for the bonding of almost 60% (except for Cu) of traffic-related HMs. The strong correlations between the Fe content and other traffic-related HMs (Table 3) allow us to suppose that iron species can be used to indirectly estimate the content of HMs. Consequently, the strong magnetic properties of iron species and their significant contents in street dust could contribute to a strong magnetic signal that can be easily detectable by magnetic methods. According to a study on dust generated by vehicle traffic on an expressway (Świetlik et al., 2015), the F(3) fraction included goethite, magnetite, and Fe released from gray cast iron and partially from brake block material (metallic iron), whereas crystalline hematite and the majority of metallic iron from brake block formed the F(5) fraction. The greater chemical resistance of metallic iron (about 60%) in the F(5) fraction was postulated on the basis of the chemical fractionation of a

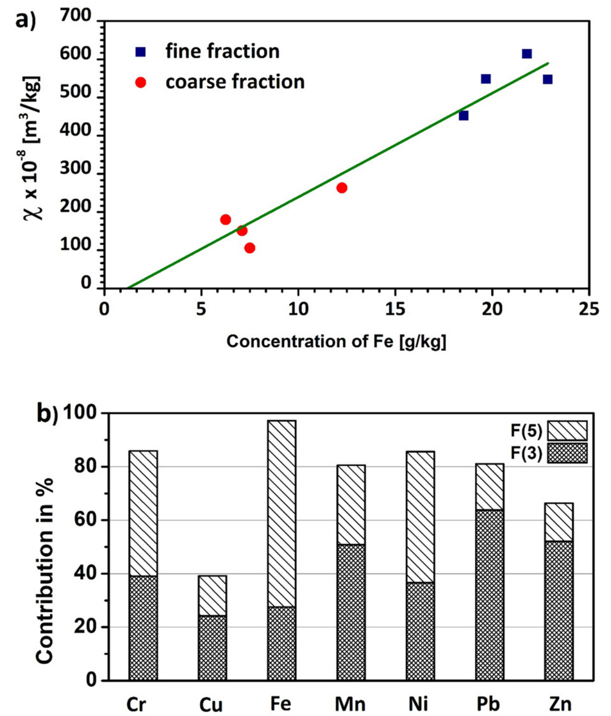

Fig. 3 – (a) Linear relation between the concentration of iron and magnetic susceptibility (χ) (Pearson's coefficient r=0.98, p<0.001); (b) average contribution of traffic-related heavy metals to reducible F(3) and residual F(5) chemical fractions of street dust.

brake block composite material and traffic-related metals and their compounds in road dust (Świetlik et al., 2015). This finding allows inferring that strong magnetic iron oxides, such as magnetite included mainly in the F(3) fraction, can contribute more significantly to magnetic susceptibility than iron compounds such as hematite and/or other Fe compounds with weak magnetic properties.

2.3. *Identification and characterization of iron magnetic phases in street dust*

2.3.1. *Mössbauer spectrometry outcomes*

Room-temperature transmission Mössbauer spectra obtained for selected samples are presented in **Fig. S3**. The exemplary transmission Mössbauer spectrum for P-IA sample recorded at room temperature is presented on the left side of Fig. 4. Each spectrum was fitted with a set of 10 components: G01–G10 (both Zeeman sextets and quadrupolar doublets). The mineralogical specification found with MS is detailed in Table 4. It should be stressed that all contributions of iron determined from the Mössbauer spectra were in fact the relative amounts in a given mineralogical phase with respect to the total content of iron in the sample. This regularity was well met if Debye–Waller factors were similar for all phases.

Iron speciation in the street dust samples based on the MS results is shown in Fig. 5. The first category comprised magnetic oxides (i.e. ferrimagnetic magnetite-possibly with maghemite-and antiferromagnetic hematite), the second

Table 4 – The specification of the components fitted to the Mössbauer spectra (FM – ferromagnetic/ferrimagnetic, AFM – antiferromagnetic, PM – paramagnetic, SPM – superparamagnetic)

Label	Form	Corresponding iron site
G01	sextet	hematite AFM
G02	sextet	magnetite (oxidized) - A site of Fe (tetrahedral) + maghemite FM
G03	sextet	magnetite (oxidized) - B site of Fe (octahedral) FM
G04	sextet	goethite AFM
G05	sextet	alpha-Fe (ferromagnetic), ferrite from steel FM
G06	sextet	carbides from steel FM
G07	doublet	main Fe^{3+} site in aluminosilicates PM + fine grains of goethite SPM
G08	doublet	other Fe^{3+} site in aluminosilicates PM
G09	doublet	other Fe^{2+} site in aluminosilicates PM
G10	doublet	main Fe^{2+} site in aluminosilicates PM

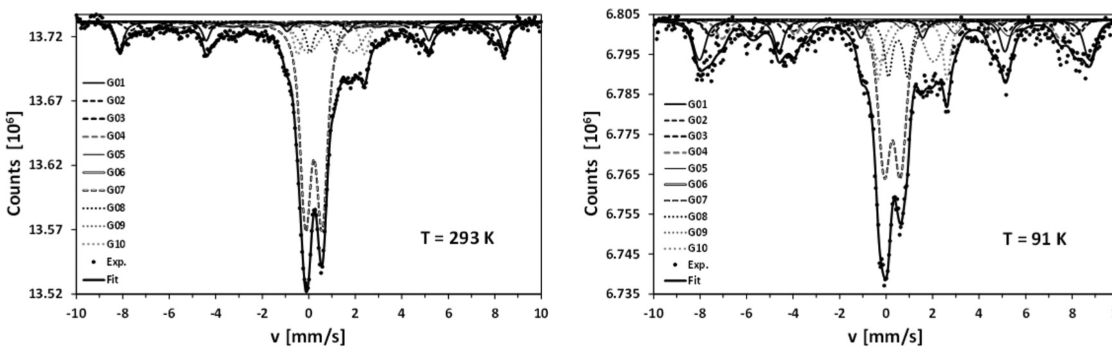

Fig. 4 – Comparison of ^{57}Fe transmission Mössbauer spectra for P-IA sample (fine fraction from site I) recorded at room temperature and near-LN temperature, respectively.

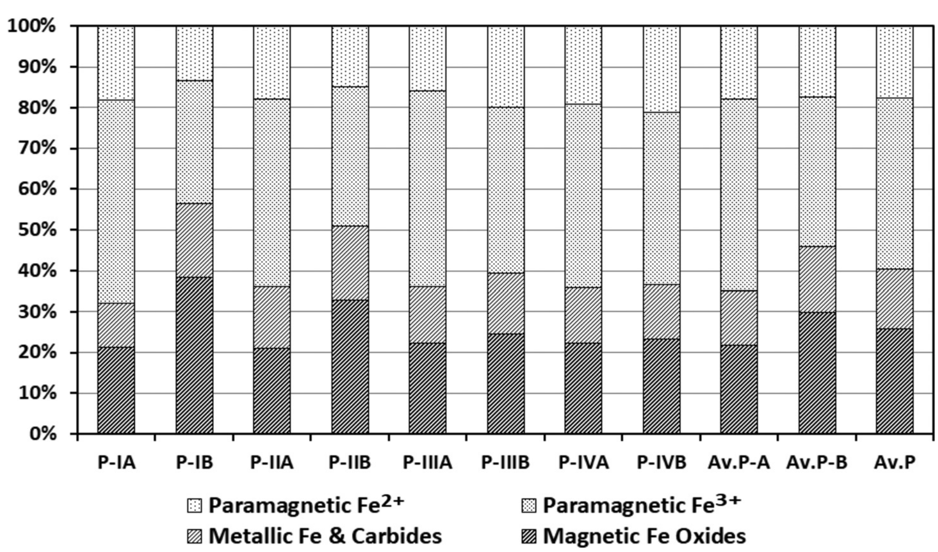

Fig. 5 – Partitioning of iron in the street dust samples by the ^{57}Fe transmission Mössbauer spectrometry method. The graph also presents the average iron distribution pattern for both sieve fractions and all samples.

comprised metallic iron, carbides, and possibly goethite (all magnetically ordered), the third and fourth ones comprised the paramagnetic iron Fe^{3+} and Fe^{2+} (belonging mostly to the aluminosilicates). Due to the soil-based origin of the samples, the last two paramagnetic-type categories were dominating; nevertheless, the relative abundances of magnetic iron oxides were high enough (20%–30%) to state that the samples originated from the street dust strongly influenced by anthropogenic activity. The most pronounced feature seems to be the fact that the relative contributions of all distinguished phase categories were almost the same for all samples of fine fractions collected from different locations. This leads to

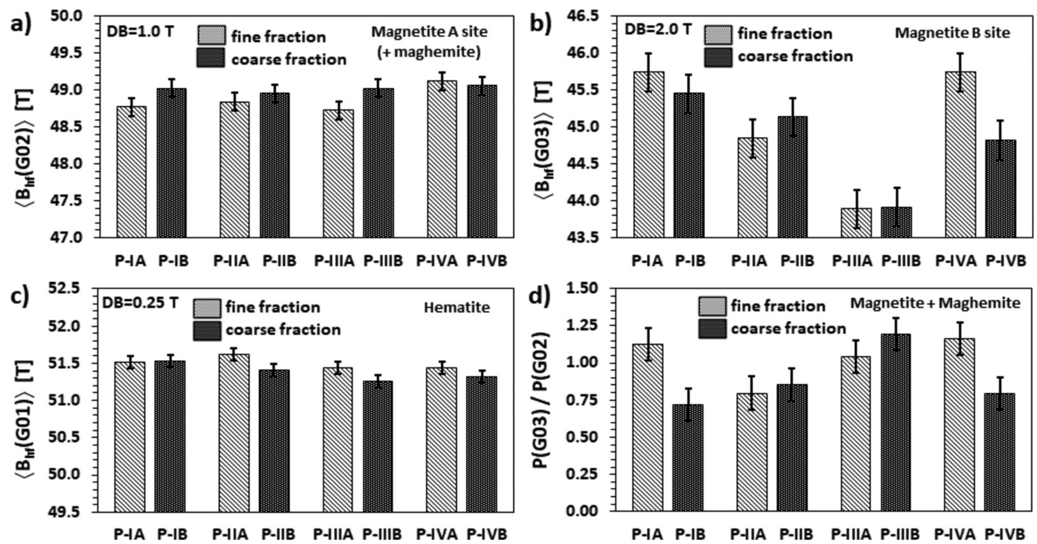

Fig. 6 – Fitted hyperfine field mean values of (a) G02 component (magnetite A site+maghemite), (b) G03 component (magnetite B site), and (c) G01 component (hematite) for all samples. The error bars indicate the statistical uncertainties of fitting mean values. The DB quantity is a half-width of Gaussian-like hyperfine field distribution. Graph (d) represents the ratio of the contribution of G03 component to the contribution of G02 component, which corresponds to the ratio of B site to A site contributions in magnetite perturbed with defects and the presence of maghemite.

the conclusion that fine fractions are more homogeneous and less sensitive to local influencing factors of incidental origin. These findings also agree well with the results of chemical fractionation.

The further detailed analysis of hyperfine parameters and contributions of individual components in the Mössbauer spectra provided valuable information on the subtle differences found in the structure and mineralogy of the investigated street dust samples. In Fig. 6**a**, it can be seen that the fitted mean values of the hyperfine fields $<B_{hf}>$ for G02 component (tetrahedral A site of Fe in magnetite and possibly in maghemite) are compared for all the samples. This component was fitted with a hyperfine field Gaussian distribution of half-width DB of 1 T. The mean values obtained for the samples belonging to the fine-grained fraction from the first three locations (P-IA, P-IIA, and P-IIIA) were slightly lower than those from the coarse fraction (P-IB, P-IIB, and P-IIIB). It could be a sign of spin-relaxation effects (superparamagnetism) of possible finer magnetic cores of the grains; however, it is only a probable, but not a conclusive statement, due to the fact the differences in hyperfine fields are not much bigger than the statistical uncertainty of fitting. The hyperfine fields corresponding to the octahedral B site in magnetite (component G03, Fig. 6**b**) did not reveal a similar correlation, presumably due to their greater sensibility to the structural defects in the crystalline lattice. Moreover, the statistical uncertainties of $<B_{hf}$(G03)$>$, as well as the half-width of the distribution, are larger than for G02 component, and thus no reliable tendencies could be found. In the case of hematite (component G01, Fig. 6**c**), one can conclude that $<B_{hf}$(G01)$>$ was almost identical for all the samples within a very small statistical uncertainty (and considering very narrow distribution).

The ratio κ of iron contribution in B site to that in A site is considered as a good indicator of magnetite nonstoichiometry. For ideal, stoichiometric magnetite, this proportion is equal to 2. As seen in Fig. 6**d**, the κ=P(G03)/P(G02) ratio took very low values, close to 1 or even lower. It is a pronounced sign of the considerable amount of defects in the spinel crystalline lattice of magnetite. As analyzed by Gorski and Scherer (2010) and Szumiata et al. (2017), the basic reason for lowering kappa values could be the iron vacancies ([]) in the octahedral site of the spinel structure of magnetite $[Fe^{3+}]^{Tet}[Fe^{2+}{}_{1-3\delta}Fe^{3+}{}_{1+2\delta}[]_{\delta}]^{Oct}O_4$. When the concentration δ of these vacancies is equal to ⅓, the average oxidation degree of iron reaches a maximum value of 3 and magnetite transforms to maghemite (γ-Fe_2O_3), a case corresponding to κ=5/3. Even lower values of κ could be caused by a higher concentration of iron vacancies in tetrahedral sites, but together with oxygen vacancies in order to prevent the oxidation state of iron from exceeding 3. This points to the strongly defected grains of metallurgical dust (Szumiata et al., 2017). Undoubtedly, pure maghemite does not explain the form of the observed spectra because it can be effectively represented by only one sextet. Thus, according to Fock et al. (2017), one can conclude that exceptionally low values of κ could indicate the presence of magnetite–maghemite mixture. In the Mössbauer spectra, the sextet corresponding to maghemite was described by the hyperfine parameters very similar to those of the sextet referring to A site in magnetite. Therefore, the contribution of G02 subspectrum was more or less a sum of these two components and could make κ values considerably low when the content of maghemite is high enough. When comparing Fig. 6**d** with Fig. 7**a**, a qualitative correlation between κ values and hematite content (relative to magnetite) can be noticed for the samples belonging both to the fine and coarse sieve fraction. This feature seems to be quite natural in terms of the oxidation process of magnetite. The samples characterized by revealing small κ values contained considerable

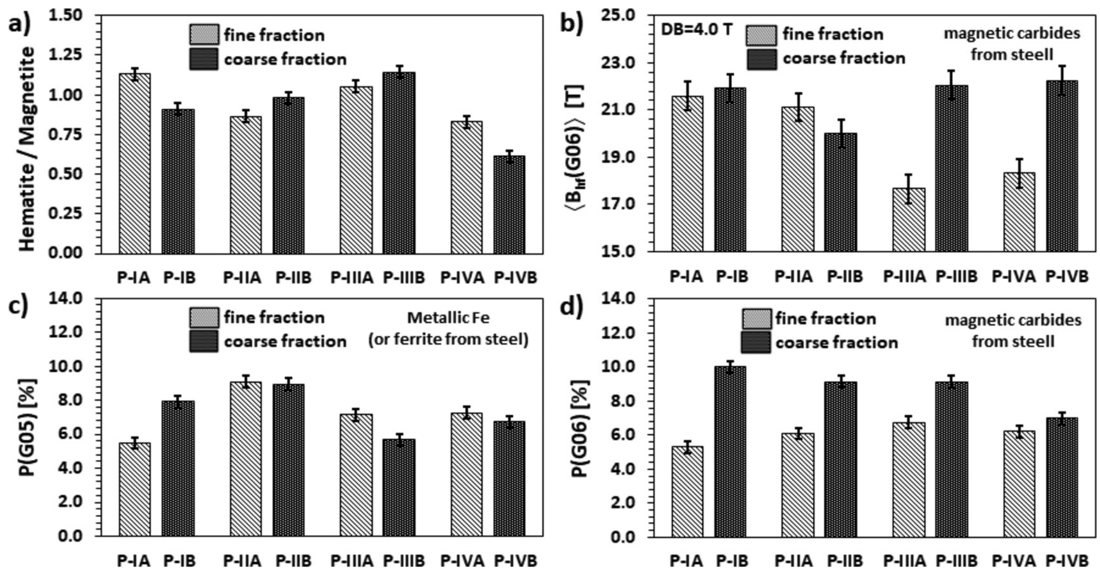

Fig. 7 – Further characteristics of magnetic components in the Mössbauer spectra. (a) hematite to maghemite contribution ratio, (b) mean hyperfine magnetic fields for the subspectra corresponding to magnetic carbides (from steel), (c) contribution of metallic iron (or ferrite phase from steel), and (d) contribution of magnetic carbides. The error bars indicate the statistical uncertainties of fitted quantities. The DB quantity is a half-width of Gaussian-like hyperfine field distribution.

amounts of maghemite (γ-Fe_2O_3) which is the first step of oxidation. In this case, the hematite (α-Fe_2O_3) content was lower because this was obtained in the next stage of the oxidation process.

The presence of metallic iron in the street dust samples seems to be a very essential question to be answered from MS. The natural soil background is influenced not only by the anthropogenic products of steel corrosion but also by the wear products originating from intense but low-speed traffic. The frequent use of braking systems in vehicles leads to the generation of a considerable amount of steel particles. Since the main constituent of many steel grades is low-carbon ferrite phase, component G05 in Mössbauer spectra was considered as a sextet of a fixed hyperfine magnetic field (HMF) of 33.0 T, which is a characteristic of metallic α-Fe. Contrary to the bulk ferrite, this component was assumed as a smeared distribution of HMF with a half-width DB of 3 T, in order to achieve a satisfactory quality of fitting. It is a natural consequence of the fine fragmentation and defectiveness of grains. As seen in Fig. 7**c**, the contribution of metallic iron was maximal for the samples (P-IIA, P-IIB) with an estimated value of about 9% with respect to the total amount of iron. Moreover, the next component, G06, in the Mössbauer spectra was added to fill the gap with HMF distribution <33.0 T. This range (Fig. 7**b**) corresponds to the ferromagnetic iron carbides (Stevens et al., 2005; Liu et al., 2016). The fitted distribution was very wide (DB=4 T), and the statistical uncertainties of the mean values were relatively huge for all samples. The contributions of G06 component (5%–10% of total Fe in the sample, Fig. 7**d**) were comparable to that of metallic iron (ferrites). This seems to be an unexpected result because typically the total abundance of carbides in steel is only several percent compared to the dominating ferritic phase. Thus, presumably the G06 component comprised not only iron carbides but also fine pieces of ferritic steel—strongly defected in wear processes accompanying the friction. Consequently, the estimated contribution of the phase related to metallic iron was well beyond 10% of the total Fe content. In fact, it is not very astonishing because fresh wear products of steel are produced constantly and systematically, and there is not enough time for their full corrosion. The MS outcomes concerning the metallic iron content are confronted with the results of magnetic methods in the Discussion section.

The values of quadrupole splitting (QS) and isomer shift (IS*, with respect to α-Fe foil) of four paramagnetic components (as doublets) for all the samples are presented in **Figs. S4a–d** and **S5a–d**. Typically, these doublets are attributed to the Fe^{3+} (low QS) and Fe^{2+} (high QS) sites of iron in the paramagnetic aluminosilicates (clays), which are common constituents of soils. As seen in the figures, the numerical uncertainties of fitting are significantly smaller than the differences in the values corresponding to the samples from different fractions and locations. It means that from the metrological point of view, the values of QS and IS determined with MS are good, reliable identifiers of natural soil background in the anthropogenically affected samples of municipal street dust. Nevertheless, a good statistical determination of hyperfine parameters is not equivalent to the quality of interpretation. In this case, still, there exist some doubts concerning the origin of the dominating doublet G07 attributed to the main Fe^{3+} site. The contribution of this component is surprisingly very high because in the majority of iron-bearing aluminosilicates there is no such disproportion between the abundances of main Fe^{3+} and Fe^{2+} sites. Thus, it cannot be excluded that a part of G07 doublet comes from the ultrafine fraction of magnetic particles. The QS(G07) value of 0.71 mm/s obtained for P-I sample is not very different from the QS value of 0.55 mm/s found by Brok et al. (2014) and Valezi et al. (2016) for the 5.7-nm particles of goethite in the vicinity of ambient temperature. Goethite (α-FeOOH), as an oxyhydroxide containing ferric Fe(III), is a common nanocrystalline mineral in nature which in bulk, crystalline form exhibits antiferromagnetic properties up to the Néel temperature of around 400 K. In the case of nanograins, the spin relaxation phenomena lead to the superparamagnetic-like state of goethite, which is recognized in the Mössbauer spectra as a doublet. To find out if such doublet contributes to component G07, the transmission MS measurement was performed at lowered temperatures. The spectrum collected for P-IA (fine fraction from the site I) sample at room temperature and at near-LN temperature, i.e. 91 K, can be compared in Fig. 4. The collected spectra differed considerably from each other. At room temperature, the dominating doublet G07 comprised over 44% of total Fe and almost 68% of Fe associated with aluminosilicates. At low temperature, the intensity of G07 doublet decreased from 44% to 28% in terms of the total iron content. Referring only to the doublets from aluminosilicates, the contribution of G07 doublet changed from 68% to 50%. Both changes point to the real, considerable evolution of this subspectrum. It should be added that the QS(G07) value at LN temperature was almost the same as at ambient temperature (0.70 mm/sec). Parallelly, the contribution of G04 sextet increased from an almost negligible value of <1% to about 8%. This component was related to goethite in the antiferromagnetic state. Its hyperfine field changed from about 37 to 45 T after a reduction in the temperature, which is in very reasonable agreement with the reference data (Murad, 1982; Stevens et al., 2005). However, it cannot be excluded that antiferromagnetic goethite also contributes to other components of lower hyperfine fields, because of the wide distribution of ultrafine grain sizes. The evolution of both of G07 and G04 components clearly confirms the hypothesis that the sample contains nanograins of goethite and their behavior changes from superparamagnetic to antiferromagnetic at near-LN temperature. It means that at room temperature the G07 doublet is undoubtedly influenced by nanogeothite contribution. Moreover, the obtained results indicate that for a reliable estimation of iron contribution belonging to aluminosilicates themselves it is necessary to perform MS analyses at reduced temperatures.

2.3.2. *Magnetic method outcomes*

In the case of magnetic methods, an appropriate approach for the identification of magnetic minerals is the measurement of magnetic hysteresis loop and thermomagnetic curves of $\kappa(T)$ and $M(T)$. The representative, high-temperature curves of $\kappa(T)$ measured for both granulometric fractions of P-II location are presented in Fig. 8. Generally, the curves for fine-grained fraction displayed very similar behavior, where a small peak in the range of 280–300°C was observed on the heating curve followed by a weak decrease and finally a wide peak starting at about 400°C. Evidently, a further decrease appeared indicating the magnetic transition from ferri- to paramagnetic phase at the Curie temperature of 580±5°C for magnetite (T_{CMg}) (Fig. 8a and b). During further heating, the value of κ reduced to nearly zero at a temperature higher than T_{CMg}. On the cooling curve, the reversed magnetic transition for magnetite was detected at a T_{CM} of ~580±5°C, and then the intensity of κ increased, suggesting the formation of a new mag-

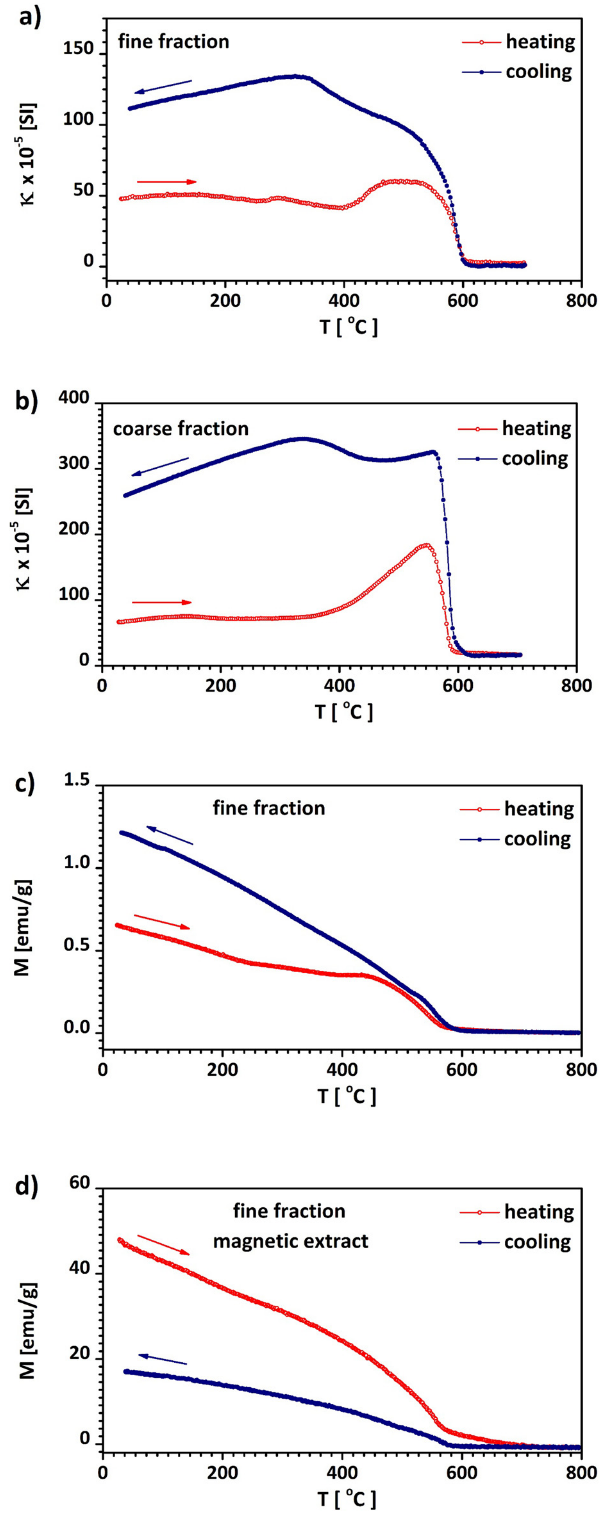

Fig. 8 – Curves of the temperature dependence of magnetic susceptibility $\kappa(T)$ for the (a) fine fraction P-IIA and (b) coarse fraction P-IIB (b) of street dust. The curve of (c) induced magnetization $M(T)$ for the fine fraction P-IIA and (d) the magnetic extract of fine fraction P-IIA. Heating curve is shown by a red line and cooling curve by a blue line.

netic phase, apparently magnetite. The systematic decrease from 400°C can be interpreted as a rearrangement in the domain structure of magnetic grains. The curves $\kappa(T)$ for coarse-grained fraction were almost identical for all the locations. On the heating curve, hardly visible fluctuations in κ up to 400°C were followed by a wide Hopkinson-like peak, before T_{CMg} was approached. On the cooling curve, a rise in the intensity of κ appeared at T_{CMg}, followed by a relatively narrow Hopkinson-like peak and a gradual drop that started at 400°C. Regardless of the granulometric fraction, the cooling curves ran above the heating ones, indicating the strong magnetic enhancement after the heating–cooling cycle. This behavior can be interpreted as the formation of new magnetite from the product arising from the thermal-activated chemical alteration of diamagnetic or/and paramagnetic minerals (Dunlop and Özdemir, 1997; Elmore et al., 2012). It is interpreted that the small peak in the range of 280–300°C resulted from the thermal alteration of Fe-rich clay minerals or conversion of poorly crystallized ferric oxides (e.g. ferrihydrite) to maghemite, which eventually transforms into hematite with weak magnetic properties (Torrent et al., 2006; Lu et al., 2012). The wide Hopkinson-like peak observed mainly for the coarse-grained fraction can suggest a wide grain-size distribution of small magnetic particles, probably in SD/pseudo-single domain (PSD) state (Dunlop and Özdemir, 2007).

The curves of M(T), measured at the temperature range of 35–800°C, confirmed magnetite as the main magnetic phase (T_{CMg}=580±5°C). The representative curves for both granulometric fractions of P-II location are presented in Fig. 8**c** and **d**. Magnetization did not reduce to zero at 600°C for the fine fraction indicating the presence of a high-temperature magnetic phase. The greater effect of a second magnetic phase was visible on the M(T) curves measured for magnetic extract (Fig. 8**d**) where the Curie temperature at T_{CFe}=770±5°C clearly corresponded to the presence of metallic iron. At temperatures <600°C, the cooling curve showed that the intensity of magnetization was decreasing, which suggests the oxidization of metallic iron to magnetite during the heating–cooling cycle. This interpretation is in coincidence with the studies of Górka-Kostrubiec (2015), Górka-Kostrubiec and Szczepaniak-Wnuk (2017), and Dytłow et al. (2019) which showed the presence of metallic iron or steel (iron-based alloys) in indoor and street dust. For all coarse-grained samples, the intensity of magnetization on the curves $M(T)$ reduced to zero >600°C, which may suggest that the second phase was undetected.

The hysteresis parameters of all the samples are listed in **Table S1**. The hysteresis loops were relatively narrow and saturated at the magnetic field of 400–500 mT. The shape of hysteresis loops was quite similar, and their coercivity parameters varied in a narrow range of Bc=8.3–11.7 mT (Fig. 9**a**) while Bcr=19.5–31.7 mT, (Fig. 9**b**) were indicative of the domination of ferrimagnetic phases in all samples.

As magnetic mineralogy is dominated by magnetite, the ratios of hysteresis parameters M_{rs}/M_s and B_{cr}/B_c presented on the Day–Dunlop plot (Dunlop 2002a, 2002b) can be a useful approach referring to the state of magnetic domains and by implication to the size of magnetic grains (SD in the size range of 0.03–0.08 µm, PSD in the size range of 0.1–20 µm, and multidomain (MD) at a size of >20 µm) (Fig. 10**a**). The data for the coarse fraction were scattered between "3" and "1" SD+MD

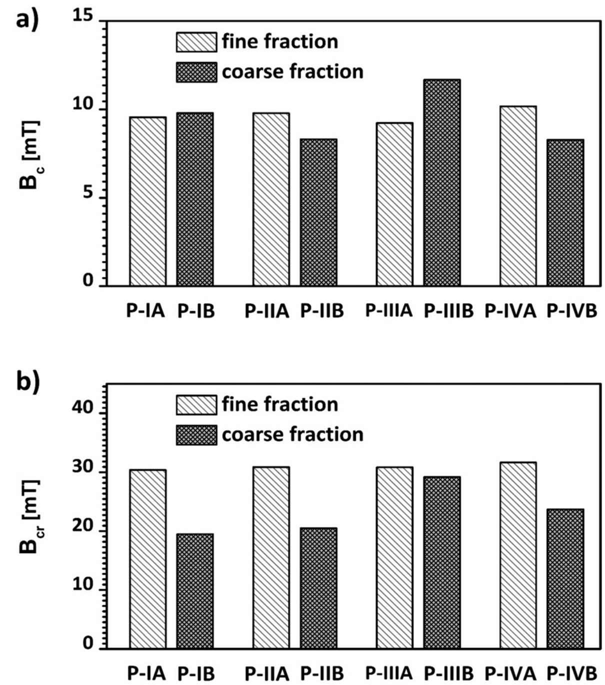

Fig. 9 – Coercivity parameters of hysteresis loop coercivity (a) and coercivity of remanence (b) for street dust collected in four sampling sites P-I, P-II, P-III, and P-IV.

mixing curves indicating the 60%–80% contribution of MD grains. The fine fraction dominated by magnetite-like phase shifted toward a slightly greater contribution of the MD grains of about 80%, and they were much clustered on the "3" mixing curve of SD+MD in the case of elongated magnetite grains. Fig. 10**b** shows the so-called "King plot" (King et al., 1982), where χ is indicative of the quantities of ferrimagnetic and incomplete antiferromagnetic minerals (Dearing et al., 1996), whereas χ_{ARM} is the magnetic-domain parameter most sensitive to SD ferrimagnetic grains (Lehndorff and Schwark, 2010). The King plot is applied in environmental magnetism to find out the presence of the grain size of the ARM-carrying grains (i.e. those showing SD properties). The average grain size inferred from the King plot was in the range of 1–5 µm corresponding to PSD magnetite which can be considered as the small MD grains exhibiting a mixture of SD-like (with high remanence) and MD-like (with low coercivity) behaviors (Moskowitz, 2007). The coarse-grained fractions (P-IB, P-IIB, and P-IVB samples) with relatively low magnetic susceptibility lay near the straight line for 5-µm grain size, whereas the fine-grained fractions (P-IA, P-IIA, P-IIIA, and P-IVA samples) exhibiting the highest magnetic susceptibility shifted toward smaller grains.

3. Discussion

Research shows that the use of three complementary methods allows identifying the composition of street dust, in terms of iron-bearing minerals, the pseudo-total concentration of HMs, and their distribution among the defined chemical frac-

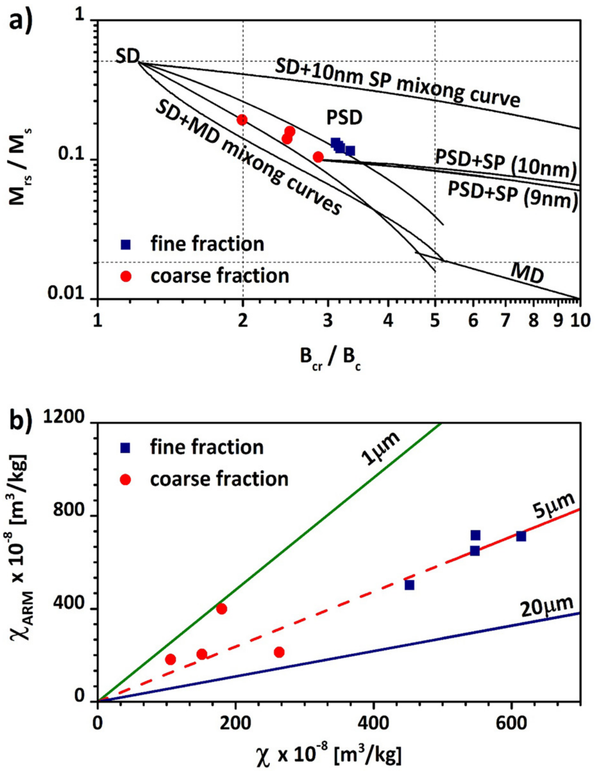

Fig. 10 – (a) Ratios of M_{rs}/M_s and B_{cr}/B_c on the Day–Dunlop plot. The red circles indicate the fine granulometric fractions, and blue circles indicate the coarse fractions of street dust. The single-domain (SD), pseudo-single domain (PSD), and multidomain (MD) regions are marked after Day (1977). The theoretically calculated mixing curves for SD+MD, PSD+SP10nm, PSD+SP9.3nm, and MD and SD+10nm SP grains in the case of magnetite are marked after Dunlop (2002a, 2002b). (b) Biplot of anhysteretic susceptibility (χ_{ARM}) versus magnetic susceptibility (χ) is shown by the so-called King plot.

tions. The MS outcomes can naturally complement the results obtained from the chemical fractionation analysis and spectroscopic elemental analysis as well as magnetic methods. Merging the data of the absolute iron concentration in the street dust samples obtained with the chemical elemental analysis (Fig. 1) with that of relative contributions of iron corresponding to the individual phases determined by MS (Fig. 5), one can estimate the content of iron-bearing minerals. Moreover, a comparison of the relative contributions of the Fe-bearing phases determined with MS and the chemical fractionation method broadens the knowledge on the chemical content and structure of street dust. Chemical fractionation enables classifying the iron mineralogical phases based on their stability in the environmental condition. The distribution of iron in street dust included four mineral fractions, among which the residual fraction and reducible fraction predominated (Fig. 1). MS offers other possibilities, instead of the determination of chemical fractions; it allows detecting individual minerals (Table 4) and even the abundances of iron ions in different crystallographic positions in the given minerals. The iron in ferro-/antiferromagnetic oxides can be easily resolved from the ferric (Fe^{3+}) and ferrous (Fe^{2+}) ions in iron-bearing paramagnetic minerals. As shown by the MS results, the stoichiometry of magnetite, as well as the abundance ratio of hematite to magnetite, is a very good and specific signature of the environmental samples influenced by anthropogenic activity. In general, and in the case of the street dust samples investigated here, MS allows an additional characterization of the samples by use of hyperfine parameters. It has been shown that subtle differences in the hyperfine field, QS and isomer shift of iron species, determined with spectroscopic precision, can be the fingerprints of individual samples, describing the structural details and defects both of anthropogenic component and natural soil background.

Regardless of the grain size of the fraction, street dust was dominated by a magnetite-like phase, which was clearly detected by both MS and magnetic methods. The hyperfine parameters of two individual sextets G(2) and G(3) (Table 4) contributing to the Mössbauer spectra were an attribute of the magnetite-like phase. However, exceptionally low values of P(G03)/P(G02) ratio may indicate more of a mixture of magnetite and maghemite resulting from the partial oxidation of magnetite to maghemite. The apparent purity of magnetite is confirmed by thermomagnetic curves (Fig. 8) indicating the Curie point at ~580°C. The fact that the Curie temperature is almost identical to that of pure magnetite can be explained by the partial oxidation of magnetite grains that at last contain the magnetite core surrounded by a concentric layer of maghemite (Cui et al., 1994). Roberts et al. (2018) reported that oxidation at a low temperature causes the reduction, among others, of magnetic susceptibility, saturation magnetization, and remanence, but an increase of coercivity. For the studied street dust samples, the values of coercivity between 8.3 and 11.7 mT were in the range for the PSD grains of pure magnetite (32 mT for the grain size of 0.6 µm and 6.5 mT for 20 µm) (Dunlop, 2014).

The component G01 recognized as hematite was the second, next to magnetite, iron oxide found in all the analyzed street dust samples. Despite the small contribution (5%–10%), hematite seems to be a typical component of traffic-related dust, which can be relatively easily identified by MS and hardly ever found using magnetic methods. This discrepancy can be explained by the fact that the low relative contribution of hematite in a mixture with a dominant amount of magnetite is almost impossible to detect in the κ(T) curves by the Curie punt as well as by constriction of the hysteresis loop typical of the coexistence of hematite with a magnetic phase differing in coercivity. The M_s of the magnetite powder is 150 times higher than that of the hematite powder, and the magnetic susceptibility of bulk magnetite is 670 times higher compared to hematite. Frank and Nowaczyk (2008) reported that to observe a significant influence of hematite on the magnetic parameters, its contribution to the mixture with magnetite must exceed 95%.

An important achievement of the MS study was the confirmation of the presence of metallic iron in street dust. In this study, the presence of metallic iron (iron-rich phases from steel, iron carbides) is considered as an indicator of anthropogenic activity—especially of traffic-related sources. It was determined together with other iron minerals in the F(3) fraction by chemical fractionation method by Świetlik et al. (2015). The results of MS analysis demonstrated that the contribution of metallic ion is not negligible, ranging from 5 to 10%. Identification of such a small contribution of metallic iron in the street dust was not easy because of imperfect statistics of the spectra and smeared lines. However, the correctness of the interpretation was supported by the outcomes of thermomagnetic measurements. The presence of metallic iron was also demonstrated by a nonzero signal above 600°C on the heating curve of M(T) (**Fig. 8d**) and by the Curie temperature at about 760°C (Górka-Kostrubiec et al., 2019).

The presence of goethite in the investigated street dust samples was also confirmed by the Mössbauer spectra. Goethite is one of the few natural minerals, which usually takes the form of ultrafine grains in a nanometric range. In fact, a part of goethite was large-grained (antiferromagnetically ordered) and another was fine-grained (Murad, 1982; Vandenberghe et al., 2000). Due to the spin-relaxation phenomena at room temperature, the latter fraction was represented in the Mössbauer spectra as a "paramagnetic" doublet that was practically indistinguishable from the dominating Fe^{3+}-like doublet related to the aluminosilicates (Kierlik et al., 2020). As proved by the MS results, an effective way to determine the real contribution of goethite is to measure the spectra at LN temperature. Within the standard interpretation of the Mössbauer spectra measured at room temperature, one always tends to overestimate the contribution of the aluminosilicates-rich fraction and underestimate the contribution of the "magnetic" fraction.

A combination of the two interpretation tools of magnetic results, including the Day–Dunlop diagram and the King diagram, resulted in surprisingly similar findings describing the domain structure of magnetite grains. It was found that the magnetic fraction was dominated by a mixture of small MD and SD grains, the average size of which was in the range of 1–5 µm. Moreover, regardless of the location, the fine granulometric fraction of street dust was strongly enriched in AMPs showing a quite homogeneous domain structure with an average grain size of about 5 µm.

Many experimental studies (Bourliva et al., 2016; Wang et al., 2019) have shown that AMPs are associated or co-occur with HMs, while magnetic susceptibility as well as M_s and M_{rs}, which approximate the concentration of magnetic carriers, can be used for quickly assessing the level of air and soil pollution. The sequential extraction method used for street dust can reveal the iron-bearing fractions that are responsible for a magnetic signal. Our research shows that iron was mainly associated with the reducible and residual fraction. This seems understandable if we consider the reducible fraction F(3) as carrying mainly strong magnetic iron oxides (magnetite/maghemite), while the residual fraction F(5), apart from a minor amount of metallic iron (steel or its alloys), is mainly formed by weak magnetic oxide (i.e. hematite and iron compounds with paramagnetic properties). The doublets observed in the Mössbauer spectra are an attribute of the Fe^{3+} (low QS) and Fe^{2+} (high QS) sites of iron in the paramagnetic aluminosilicates, the share of which was estimated to be around 60% compared to all Fe-containing phases.

The precise determination of iron speciation is important not only from the view of general cognitive incentives but also due to the direct link of AMPs to the content of HMs, which are considered the main pollutants introduced into the environment by street dust. Thus, the HMs mainly distributed in F(3) and F(5) fractions bonding over 95% of iron should correlate well with the concentration of AMPs, and consequently with magnetic susceptibility. It was found that the share of reducible fraction of HMs decreased in the order: Pb>Zn>Mn>Cr>Ni>Fe>Cu, while in the case of the residual fraction of HMs their shares formed the order, Fe>Ni>Cr>Mn>Pb>Cu>Zn. Hence, it should be expected that this is a contribution scheme of traffic-related HMs associated with Fe-bearing magnetic phases in street dust.

The last aspect of our research is the negative health effect resulting from HM toxicity. The study showed that a quantitative assessment of only the pseudo-total concentration of HMs appears to be insufficiently precise. This approach does not provide a reliable and realistic insight into the toxicity of metals to both the environment and human health. For a reliable assessment, it is necessary to engage a more precise approach, by applying chemical fractionation to reveal the speciation of HMs in dust. The recognition of the chemical forms that transfer HMs is the key to indicate which metals are the most chemically mobile and bioavailable in a given type of dust. In the study by Jan et al. (2018), two chemical fractions, namely water-soluble and exchangeable, were considered environmentally mobile and bioavailable. The results of the present study show that the share of water-soluble fraction in street dust was negligible, while the weak acid-soluble fraction carried mainly three metals: Zn (56.9%), Mn (31.6%), and Cu (6.3%). The high amount of Zn in street dust is related to the addition of ZnO and ZnS to the tire during the vulcanization process (Smolders and Degryse, 2002; Ozaki et al., 2004). The reducible and oxidizable fractions are considered as less mobile and bioavailable; however, they exhibit long-term effects on the environment and human health. In the street dust samples examined, four HMs, namely Cu, Pb, Mn, and Zn, were found to make a significant contribution to F(3) and (F4) fractions (**Fig. 1**) and thus seemed to have a potentially toxic effect on the environment. Pb is an extremely toxic HM that disturbs various plant physiological processes, and in the human body, it mainly penetrates into the central nervous system and the gastrointestinal tract (Jaishankar et al., 2014). In turn, Cu can be an externally toxic metal when ingested by humans. It should be emphasized that the two potentially dangerous metals, Ni and Cr, are bound in the street dust with the residual fraction, which is the most persistent in the environment and the least mobile.

4. Conclusions

Integration of chemical fractionation, MS, and magnetic methods proved useful in identifying iron-containing phases as well as chemical fractions of traffic-related HMs favored by Fe-bearing phases in street dust. The most important outcomes of the research can be summarized as follows.

The fine-grained fraction with an average diameter of <63 µm was the most enriched in traffic-related HMs such as Zn, Pb, Fe, Cu, Cr, Ni, and Mn. Consequently, the PLI assessing the total degree of HM contamination was over 2–3 times higher for the fine-grained fraction (PLI=5.0–5.9) compared to the coarse-grained fraction (PLI=1.1–1.8).

Two chemical fractions, residual and reducible, bound over 95% of the total concentration of Fe and predominantly HMs. The scheme of the contribution of traffic-related HMs to Fe-bearing chemical fraction was as follows: Pb>Zn>Mn>Cr>Ni>Fe>Cu for F(3) and Fe>Ni>Cr>Mn>Pb>Cu>Zn for F(5).

The magnetic and Mössbauer outcomes revealed the existence of several magnetic phases in street dust. The signature of the anthropogenic origin of street dust is the presence of strongly nonstoichiometric and defected grains of magnetite, the porous surface of which could be good carriers for the propagation of HMs. Admixture of magnetite with maghemite is also possible, along with a significant contribution of hematite, which was easily detected by MS. The presence of metallic iron and iron carbides in the investigated street dust samples was found as a feature distinguishing them from industrial fly ashes. The relative abundances of iron associated with individual phases were very similar for all samples belonging to the fine-granulometric fraction, which confirms its better homogeneity. Cryogenic Mössbauer measurements revealed that room temperature analysis itself leads to an overestimation of the contribution of soil-based aluminosilicates and an underestimation of the content of fine-grained goethite. The hyperfine parameters of the Mössbauer subspectra are good signatures of both anthropogenic (mostly strongly magnetic) and natural components (paramagnetic) of the samples from a definite location.

Magnetic measurements seem to be especially efficient in the screening test of the environmental samples as well as provide value-added information on the chemical composition and mineralogical/domain structure of magnetic particles incorporated in the dust. Both mineral composition and domain structure of magnetic particles are useful features for determining the anthropogenic activities that give rise to pollution, together with the magnetic particles that are typical of these sources.

Acknowledgments

This work was supported in part by the statutory grant 3179/25/P—DBUPB/2015/063 and by research work No. 3522/182/P realized in University of Technology and Humanities in Radom and by statutory activities No. 3841/E-41/S/2022 of the Ministry of Science and Higher Education of Poland.

The authors of the article express their gratitude to Prof. Jean-Marc Grenèche (Le Mans Université, France, CNRS, IBAME) for his fruitful discussion which helped in the interpretation of the Mössbauer spectra at LN temperature. We also thank Translmed Publishing Group (Cedar Hill, TX, USA), a proofreading and copyediting company, for helping in copyediting this manuscript.

Appendix A Supplementary data

Supplementary material associated with this article can be found, in the online version, at doi:10.1016/j.jes.2022.02.015.

REFERENCES

Adamiec, E., Jarosz-Krzemińska, E., Wieszała, R., 2016. Heavy metals from non-exhaust vehicle emissions in urban and motorway road dusts. Environ. Monit. Assess. (369) 188. doi:10.1007/s10661-016-5377-1.

Adamiec, E., 2017. Road environments: Impact of metals on human health in heavily congested cities of Poland. Int. J. Environ. Res. Public Health 14 (697). doi:10.3390/ijerph14070697.

Airly, https://airly.eu/map/pl, Accessed 19 October 2020.

Banerjee, A.D.K., 2003. Heavy metal levels and solid phase speciation in street dusts of Delhi. India. Environ. Pollut. 123, 95–105.

Bogusz, P., Brzózka, K., Górka, B., Szumiata, T., Woźniak, M., Gałązka-Friedman, J., 2018. Classification of meteorites - Mössbauer comparative studies of three ordinary chondrites measured in different laboratories. Acta Phys. Pol. 134, 1070–1075. doi:10.12693/APhysPolA.134.1070.

Bourliva, A., Papadopoulou, L., Aidona, E., 2016. Study of road dust magnetic phases as the main carrier of potentially harmful trace elements. Sci. Total Environ. 553, 380–391.

Brok, E., Frandsen, C., Madsen, D.E., Jacobsen, H., Birk, J.O., Lefmann, K., et al., 2014. Magnetic properties of ultra-small goethite nanoparticles. J. Phys. D: Appl. Phys. 47, 365003. doi:10.1088/0022-3727/47/36/365003, 13pp.

Christoforidis, A., Stamatis, N., 2009. Heavy metal contamination in street dust and roadside soil along the major national road in Kavala's region, Greece. Geoderma 151, 257–263. doi:10.1016/j.geoderma.2009.04.016.

Czarnowska, K., 1996. Total content of heavy metals in parent rocks as reference background levels of soils. Soil Sci. Ann. 47, 43–50 in Polish.

Cui, Y.L., Verosub, K.L., Roberts, A.P., 1994. The effect of maghemitization on large multi-domain magnetite. Geophys. Res. Lett. 21, 757–760. doi:10.1029/94GL00639.

Day, R., Fuller, M., Schmidt, V.A., 1977. Hysteresis properties of titanomagnetites: Grain-size and compositional dependence. Phys. Earth Planet. Inter. 13 (4), 260–267. doi:10.1016/0031-9201(77)90108-X.

Dearing, J.A., Dann, R.J.L., Hay, K., Lees, J.A., Loveland, P.J., Maher, B.A., et al., 1996. Frequency-dependent susceptibility measurements of environmental materials. Geophys. J. Int. 124, 228–240.

Dunlop, D.J., Özdemir, Ö., 2007. Magnetizations in Rocks and Minerals. [In:] Schubert, G., Kono, M. (Eds.), Treatise on Geophysics. Vol. 5, Geomagnetism, Academic Press Elsevier Science, pp. 311–331.

Dunlop, D., Özdemir, Ö., 1997. Rock Magnetism: Fundamentals and Frontiers. Cambridge University Press doi:10.1017/CBO9780511612794.

Dunlop, D.J., 2002a. Theory and application of the Day plot (Mrs/Ms versus Hcr/Hc) 1. Theoretical curves and tests using titanomagnetite data. J. Geophys. Res. Solid Earth 107. doi:10.1029/2001JB000486, EPM 4-1 – EPM 4-22.

Dunlop, D.J., 2002b. Theory and application of the Day plot (Mrs/Ms versus Hcr/Hc) 2. Application to data for rocks, sediments, and soils. J. Geophys. Res. Solid Earth 107. doi:10.1029/2001JB000487, 5-1 –5-15.

Dunlop, D.J., 2014. High-temperature susceptibility of magnetite: a new pseudo-single-domain effect. Geophys. J. Int. 199 (2), 707–716. doi:10.1093/gji/ggu247.

Dytłow, S., Winkler, A., Górka-Kostrubiec, B., Sagnotti, L., 2019. Magnetic, geochemical and granulometric properties of street dust from Warsaw (Poland). J. Appl. Geophy. 169, 58–73.

Elmore, R.D., Muxworthy, A.R., Aldana, M.Elmore, R.D., Muxworthy, A.R., Aldana, M. (Eds.), 2012. Remagnetization and

chemical alteration of sedimentary rocks. Remagnetization and Chemical Alteration of Sedimentary Rocks 371, 1–21.
Fock, J., Bogart, L.K., González-Alonso, D., Espeso, J.I., Hansen, M.F., Varón, M., et al., 2017. On the 'centre of gravity' method for measuring the composition of magnetite/maghemite mixtures, or the stoichiometry of magnetite-maghemite solid solutions, via 57Fe Mössbauer spectroscopy. J. Phys. D: Appl. Phys. 50, 265005. doi:10.1088/1361-6463/aa73fa, (16pp).
Frank, U., Nowaczyk, N.R., 2008. Mineral magnetic properties of artificial samples systematically mixed from haematite and magnetite. Geophys. J. Int. 175 (2), 449–461. doi:10.1111/j.1365-246x.2008.03821.x.
Gope, M., Masto, R.E., George, J., Balachandran, S., 2018. Tracing source, distribution and health risk of potentially harmful elements (PHEs) in street dust of Durgapur. India. Ecotox. Environ. Safe 154, 280–293.
Gorski, Ch.A., Scherer, M.M., 2010. Determination of nanoparticulate magnetite stoichiometry by Mössbauer spectroscopy, acidic dissolution, and powder X-ray diffraction: A critical review. Am. Miner. 95, 1017–1026. doi:10.2138/am.2010.3435 1017.
Górka-Kostrubiec, B., 2015. The magnetic properties of indoor dust fractions as markers of air pollution inside buildings. Building and Environment 90, 186–195.
Górka-Kostrubiec, B., Szczepaniak-Wnuk, I., 2017. Magnetic study of a mixture of magnetite and metallic iron in indoor dust samples. Air Qual. Atmos. Health 10, 105–116.
Górka-Kostrubiec, B., Werner, T., Dytłow, S., Szczepaniak-Wnuk, I., Jeleńska, M., Hanc-Kuczkowska, A., 2019. Detection of metallic iron in urban dust by using high-temperature measurements supplemented with microscopic observations and Mössbauer spectra. J. Appl. Geophys. 166, 89–102.
Grigoratos, T., Martini, G., 2015. Brake wear particle emissions: a review. Environ. Sci. Pollut. Res. 22, 2491–2504.
GUS Report, 2018. Statistical Offices in Warszawa. Statistical Vademecum of Regional Civil Servant, Radom city. https://warszawa.stat.gov.pl/vademecum/vademecum_mazowieckie/portrety_miast/miasto_radom.pdf (in Polish). Accessed 19 October 2020.
Harrison, R.M., Jones, A.M., Gietl, J., Yin, J., Green, D.C., 2012. Estimation of the contributions of brake dust, tire wear, and resuspension to nonexhaust traffic particles derived from atmospheric measurements. Environ. Sci. Technol. 46 (12), 6523–6529. doi:10.1021/es300894r.
Hwang, H.-M., Fiala, M.J., Park, D., Wade, T.L., 2016. Review of pollutants in urban road dust and stormwater runoff: part 1. Heavy metals released from vehicles. Int. J. Urban Sci. 5934, 1–27. doi:10.1080/12265934.2016.1193041.
Jadhav, S.P., Sawant, S.H., 2019. A review paper: development of novel friction material for vehicle brake pad application to minimize environmental and health issues. Materials Today: Proceedings 19 (2), 209–212. doi:10.1016/j.matpr.2019.06.703.
Jaishankar, M., Tseten, T., Anbalagan, N., Mathew, B., Beeregowda, K., 2014. Toxicity, mechanism and health effects of some heavy metals. Interdiscip. Toxicol. 7, 60–72.
Jan, R., Roy, R., Yadav, S., Satsangi, P.G., 2018. Chemical fractionation and health risk assessment of particulate matter-bound metals in Pune, India. Environ. Geochem. Health 40, 255–270.
Keshavarzi, B., Tazarvi, Z., Rajabzadeh, M.A., Najmeddin, A., 2015. Chemical speciation, human health risk assessment and pollution level of selected heavy metals in urban street dust of Shiraz, Iran. Atmos. Environ. 119, 1–10.
Khanal, R., Furumai, H., Nakajima, F., 2014. Toxicity assessment of size-fractionated urban road dust using ostracod Heterocypris incongruens direct contact test. J. Hazard. Mater. 264, 53–64. doi:10.1016/j.jhazmat.2013.10.058.
Kierlik, P., Hanc-Kuczkowska, A., Rachwał, M., Męczyński, R., Matuła, I., 2020. Application of Mössbauer spectroscopy for identification of iron-containing components in upper Silesian topsoil being under industrial anthropopressure. Materials 2020 (13), 5206. doi:10.3390/ma13225206.
King, J., Banerjee, S.K., Marvin, J., Özdemir, Ö., 1982. A comparison of different magnetic methods for determining the relative grain size of magnetite in natural materials: some results from lake sediments. Earth Planet. Sci. Lett. 59 (2), 404–419. doi:10.1016/0012-821x(82)90142-x.
Lee, P.-K., Yu, Y.-H., Yun, S.-T., Mayer, B., 2005. Metal contamination and solid phase partitioning of metals in urban roadside sediments. Chemosphere 60, 672–689.
Li, H., Shi, A., Zhang, X., 2015. Particle size distribution and characteristics of heavy metals in road-deposited sediments from Beijing Olympic Park. J. Environ. Sci. 32, 228–237. doi:10.1016/j.jes.2014.11.014.
Lehndorff, E., Schwark, L., 2010. Biomonitoring of air quality in the Cologne Conurbation using pine needles as a passive sampler – part III: major and trace elements. Atmos. Environ. 44 (24), 2822–2829.
Li, H.H., Chen, L.J., Yu, L., Guo, Z.B., Shan, C.Q., Lin, J.Q., et al., 2017. Pollution characteristics and risk assessment of human exposure to oral bioaccessibility of heavy metals via urban street dusts from different functional areas in Chengdu. China. Sci. Total Environ. 586, 1076–1084.
Li, X.D., Poon, C.S., Liu, P.S., 2001. Heavy metal contamination of urban soils and street dusts in Hong Kong. Appl. Geochem. 16, 1361–1368.
Liu, X., Zhao, S., Meng, Y., Peng, Q., Dearden, A., Huo, C., et al., 2016. Mössbauer spectroscopy of iron carbides: from prediction to experimental confirmation. Sci. Rep. 6, 26184. doi:10.1038/srep26184.
Lu, S.G., Zhu, L., Yu, J.Y., 2012. Mineral magnetic properties of Chinese paddy soils and its pedogenic implications. Catena 93, 9–17.
Maher, B.A., 1998. Magnetic properties of modern soils and Quaternary loessic paleosols: paleoclimatic implications. Palaeogeogr. Palaeoclimat. Palaeoecol. 137 (1-2), 25–54. doi:10.1016/S0031-0182(97)00103-X.
Mordak, R., Tetlak, M., Rawski, J., 2008. Strategy of the Development of the Radom city for the Period 2008-2020. WYG International, Warszawa http://www.radom.pl/data/other/strategia_rozwoju_miasta_radomia_na_lata.pdf (in Polish). Accessed 19 October 2020.
Moskowitz, B., 2007. Hitchhiker's Guide to Magnetism. http://www.irm.umn.edu/hg2m/hg2m.pdf, Accessed 30 March 2019.
Murad, E., 1982. The characterization of goethite by Mössbauer spectroscopy. Am. Mineral. 67, 1007–1011.
Muxworthy, A.R., Schmidbauer, E., Petersen, N., 2002. Magnetic properties and Mössbauer spectra of urban atmospheric particulate matter: a case study from Munich. Germany. Geophys. J. Int. 150, 558–570.
Ozaki, H., Watanabe, I., Kuno, K., 2004. Investigation of the heavy metal sources in relation to automobiles. Water Air Soil Pollut 157, 209–223.
Padoan, E., Romè, C., Ajmone-Marsan, F., 2017. Bioaccessibility and size distribution of metals in road dust and roadside soils along a peri-urban transect. Sci. Total Environ. 601-602, 89–98. doi:10.1016/j.scitotenv.2017.05.180.
Petrovský, E., Kapička, A., 2006. On determination of the Curie point from thermomagnetic curves. J. Geophys. Res. Solid Earth 111 (B12). doi:10.1029/2006JB004507.
Ramos, L., Hernandez, M., Gonzales, J., 1994. Sequential fractionation of copper, lead, cadmium and zinc in soils from Donena National Park. J. Environ. Qual. 23, 50–57.
Roberts, A.P., Zhao, X., Harrison, R.J., Heslop, D., Muxworthy, A.R., Rowan, C.J., et al., 2018. Signatures of reductive magnetic mineral diagenesis from unmixing of first-order reversal

curves. J. Geophys. Res. Solid Earth 123, 4500–4522. doi:10.1029/2018JB015706.
Shi, G., Chen, Z., Bi, C., Wang, L., Teng, J., Li, Y., et al., 2011. A comparative study of health risk of potentially toxic metals in urban and suburban road dust in the most populated city of China. Atmos. Environ. 45 (3), 764–771. doi:10.1016/j.atmosenv.2010.08.039.
Smolders, E., Degryse, F., 2002. Fate and effect of zinc from tire debris in soil. Environ. Sci. Technol. 36, 3706–3710.
Stevens, J.G., Khasanov, A.M., Miller, J.W.B., Pollak, H., Li, Z., 2005. Mössbauer Mineral Handbook, Mössbauer Effect Data Center. The University of North Carolina at Asheville, USA.
Sutherland, R.A., 2003. Lead in grain size fractions of road-deposited sediment. Environ. Pollut. 121, 229–237. doi:10.1016/S0269-7491(02)00219-1.
Sutherland, R.A., Tack, F.M., 2000. Metal phase associations in soils from an urban watershed, Honolulu, Hawaii. Sci. Total Environ 256, 103–113.
Świetlik, R., Trojanowska, M., Strzelecka, M., Bocho-Janiszewska, A., 2015. Fractionation and mobility of Cu, Fe, Mn, Pb and Zn in the road dust retained on noise barriers along expressway – A potential tool for determining the effects of driving conditions on speciation of emitted particulate metals. Environ. Pollut. 196, 404–413.
Szumiata, T., Gawroński, M., Górka, B., Brzózka, K., Świetlik, R., Trojanowska, M., et al., 2013. Chemical, magnetic and Mössbauer effect analysis of road dust from expressway. Nukleonika 58, 107–110.
Szumiata, T., Gzik-Szumiata, M., Brzózka, K., Górka, B., Gawroński, M., Świetlik, R., et al., 2015. Iron-containing phases in fly ashes from different combustion systems. Nukleonika 60, 151–154. doi:10.1515/nuka-2015-0030.
Szumiata, T., Rachwał, M., Magiera, T., Brzózka, K., Gzik-Szumiata, M., Gawroński, M., et al., 2017. Iron-containing phases in metallurgical and coke dusts as well as in bog iron ore. Nukleonika 62, 187–195. doi:10.1515/nuka-2017-0029.
Tessier, A, Campbell, P.G.C., Bisson, M., 1979. Sequential extraction procedure for the speciation of particulate trace metals. Anal. Chem. 7, 844–851.
Tomlinson, D.L., Wilson, J.G., Harris, C.R., Jeffrey, D.W., 1980. Problems in the assessment of heavy-metal levels in estuaries and the formation of a pollution index. Helgoländer Meeresunters 33, 566–575.
The programme of environmental protection against noise for the city of Radom. Appendix No. 1 to the Ordinance No. 2900/2018 of the President of the City of Radom dated 14 March 2018. http://www.radom.pl/data/newsFiles/zalacznik_nr_1.pdf (in Polish).
Thompson, R., Oldfield, F., 1986. Environmental Magnetism. doi:10.1007/978-94-011-8036-8.
Torrent, J., Barrón, V., Liu, Q.S., 2006. Magnetic enhancement is linked to and precedes hematite formation in aerobic soil. Geophys. Res. Lett. 33, L02401. doi:10.1029/2005GL024818.
Trojanowska, M., Świetlik, R., 2020. Investigations of the chemical distribution of heavy metals in street dust and its impact on risk assessment for human health, case study of Radom (Poland). Hum. Ecol. Risk Assess. 26 (7), 1907–1926.
Ure, A.M., Davidson, C.M., 2002. Chemical Speciation in the Environment. Blackwell Sci..
Valezi, D.F., Piccinato, M.T., Sarvezuk, P.W.C., Ivashita, F.F., Varalda Jr., Paesano A., et al., 2016. Goethite (a-FeOOH) magnetic transition by ESR, Magnetometry and Mossbauer. Mater. Chem. Phys. 173, 179–185. doi:10.1016/j.matchemphys.2016.01.067.
Vandenberghe, R., Barrero, C., da Costa, G., Van San, E., De Grave, E., 2000. Mössbauer characterization of iron oxides and (oxy)hydroxides: the present state of the art. Hyperfine Interact. 126, 247–259. doi:10.1023/A:1012603603203.
Wang, G., Chen, J., Zhang, W., Ren, F., Chen, Y., Fang, A., et al., 2019. Magnetic properties of street dust in Shanghai, China and its relationship to anthropogenic activities. Environ. Pollut. 255 (113214). doi:10.1016/j.envpol.2019.113214.
Yang, Y., Campbell, C.D., Clark, L., Cameron, C.M., Paterson, E., 2006. Microbial indicators of heavy metal contamination in urban and rural soils. Chemosphere 63, 1942–1952.
Yıldırım, G., Tokalıoğlu, Ş., 2016. Heavy metal speciation in various grain sizes of industrially contaminated street dust using multivariate statistical analysis. Ecotoxicol. Environ. Saf. 124, 369–376. doi:10.1016/j.ecoenv.2015.11.006.
Zhang, G., Bai, J., Zhao, Q., Lu, Q., Jia, J., Wen, X., 2016. Heavy metals in wetland soils along a wetland-forming chronosequence in the Yellow River Delta of China: levels, sources and toxic risks. Ecol. Indic. 69, 331–339.